

Contact Information Flow and Design of Compliance

Kevin Haninger, Marcel Radke, Richard Hartisch, Jörg Krüger

Abstract

The objective of many contact-rich manipulation tasks can be expressed as desired contacts between environmental objects. Simulation and planning for rigid-body contact continues to advance, but the achievable performance is significantly impacted by hardware design, such as physical compliance and sensor placement. Much of mechatronic design for contact is done from a continuous controls perspective (e.g. peak collision force, contact stability), but hardware also affects the ability to infer discrete changes in contact. Robustly detecting contact state can support the correction of errors, both online and in trial-and-error learning.

Here, discrete contact states are considered as changes in environmental dynamics, and the ability to infer this with proprioception (motor position and force sensors) is investigated. A metric of information gain is proposed, measuring the reduction in contact belief uncertainty from force/position measurements, and developed for fully- and partially-observed systems. The information gain depends on the coupled robot/environment dynamics and sensor placement, especially the location and degree of compliance. Hardware experiments over a range of physical compliance conditions validate that information gain predicts the speed and certainty with which contact is detected in (i) monitoring of contact-rich assembly and (ii) collision detection. Compliant environmental structures are then optimized to allow industrial robots to achieve safe, higher-speed contact.

1 Introduction

Manipulation aims to achieve a relative arrangement of objects, often with a desired set of contacts between them. In structured environments, this desired contact maps uniquely onto robot position, but as robots are applied in less-structured environments and to more complex tasks, the position of contact may vary. A robot which can robustly detect this contact state can improve autonomy, for example detecting contact states associated with success and failure can be used for online correction [1] or to provide a reward signal to a learning process [2].

However, contact involves discontinuities in dynamics and friction, presenting analytical and numerical challenges in

Authors affiliated with the Department of Automation at the Fraunhofer Institute für Produktionsanlagen und Konstruktionstechnik. Corresponding author email: kevin.haninger@ipk.fraunhofer.de. This project has received funding from the European Union's Horizon 2020 research and innovation programme under grant agreement No 820689 – SHERLOCK.

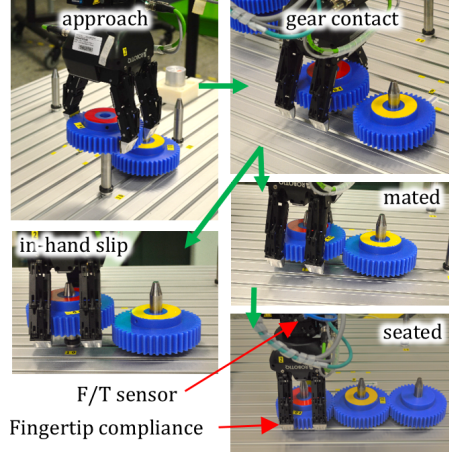


Figure 1: Contact-rich manipulation task, where a discrete collection of contact dynamics occur, corresponding to different task phases. Detecting these changes can help error monitoring like in-hand slip, and the ability to detect these changes is a function of sensor placement and physical dynamics.

modelling. A number of contact models are established [3, 4], and rigid-body contact can typically be simulated with the help of special integrators [5, 6]. Methods for model-based trajectory planning over contact continue to improve, both optimization- [7] and particle-based [8]. However, planning is open-loop, with limited error correction capacity.

As a priori contact modelling is difficult, data-based methods are often used for contact tasks. The feasibility of learning contact geometry has been shown experimentally [9] on simplified geometries, but not yet demonstrated on robotic manipulation. Alternatively, force signals can be processed by deep neural networks in an end-to-end manner [2, 10], allowing force signals to affect the control policy. This avoids problems with modelling but introduces new questions of sample efficiency and generalization [11].

Force or impedance control [12] is classical approach to contact, avoiding environment modelling by designing the robot's dynamic response to environmental input. While improving safety and often robustness, impedance control alone cannot robustly solve many complex manipulation tasks.

While advances in modelling and control are important, the capabilities which can be realized in contact are limited by hardware. The effective inertia at the contact point is critical for peak force in collision with the environment [13] and humans [14]. Physical compliance can reduce peak contact

force [15, 16] and improve contact stability [17, 18]. While reducing inertia is typically desired (to the degree possible), compliance presents trade-offs. Compliance limits the passive feedback control gain [19, 20], and reduces the effectiveness of feedforward control [21], limiting motion control performance in the sense of bandwidth and disturbance rejection.

Physical dynamics also affect the need for energy and information in contact-rich tasks. Compliance can be designed to improve energy efficiency [22], or exploited to reduce energy use [23]. Morphological computation aims to design intrinsic dynamics with ‘embodied intelligence’ [24], which has been applied to designing damping for locomotion [25]. Compliance can be optimized to reduce the need for information [26] or reduce the problem dimension [27] in manipulation tasks.

A continuous control viewpoint is often used in mechatronic design for contact, considering factors like stability, bandwidth, and peak collision force. While important, robotics also involves discrete changes – e.g., changes in contact – and the ability to infer these discrete states is also affected by hardware.

Contact task representation and monitoring by considering a discrete collection of constraints [28] or environment dynamics [29–31] is established, this paper builds on these approaches to consider how the robot dynamics and sensors affect the ability to perform this inference. Analytical rules for ‘distinguishability’ of contact state have been proposed [32], but do not consider compliance or noise. The impact of force sensor location on contact detection speed has been experimentally noted [33, §VII.C], but not analyzed.

This paper considers discrete contact states as having different coupled robot-environment dynamics, and uses a Bayesian approach to infer this given proprioceptive measurements (position and force). First, the compliant contact models are introduced, then the information gain from position and force measurements is developed in the fully- and partially-observed case. The information gain is written for a linear inertial system, and mechatronic design to optimize information transfer is considered. Finally, experiments validate that information gain predicts the certainty and speed of assembly monitoring and collision detection, where the location and degree of compliance in environmental structures is varied. The method is applied to inform the design of compliant structures to allow higher-speed contact with an industrial robot.

1.0.1 Notation

Random variables are typeset in boldface $\mathbf{n} \sim p(n)$. The normal distribution is denoted $\mathcal{N}(\mu, \Sigma)$, and $\mathcal{N}(x|\mu, \Sigma)$ denotes an evaluation of the Gaussian probability distribution function at the point x . Proportionality \propto indicates a distribution is written without a normalization constant for compactness. The matrix determinant \det can be ignored when the argument is scalar. A sequence of variables is denoted $q_{1:t} = [q_1, \dots, q_t]$.

2 Contact and robot models

This section presents the dynamic model for compliant robot contact and the observation models for position and force.

2.1 Compliant robot model

Let the robot and environment be described by generalized position $q \in Q = \mathbb{R}^D$ with time derivative \dot{q} . Compliance (in the joint, gripper, or environment) can then be modelled by adding an elastic energy term $\mathcal{K}(q) : \mathbb{R}^D \rightarrow \mathbb{R}$ to the standard manipulator Lagrangian [34], thus giving equations of motion

$$M(q)\ddot{q} + \tau(q, \dot{q}) - K(q) = B\tau_m, \quad (1)$$

where $M(q) \in \mathbb{R}^{D \times D}$ is the inertia matrix, $\tau \in \mathbb{R}^D$ contains the gravitational, Coriolis, and friction forces, spring-like forces $K(q) = \frac{d\mathcal{K}(q)}{dq} : \mathbb{R}^D \rightarrow \mathbb{R}^D$, and input matrix $B \in \mathbb{R}^{D \times K}$ modulates motor torque input $\tau_m \in \mathbb{R}^K$.

In the sequel, this model will be reduced to a two-mass model in the direction of contact motion, but provides the general statement for contact state and observations.

2.2 Contact State

A compliant contact model is used here instead of impulse-based [3] – it is assumed sufficient compliance is present to distribute the contact impulse over a longer time window. Contact is then modelled as an equality constraint over total configuration, $\phi(q) = 0$. While inequality constraints $\phi(q) \geq 0$ can capture non-penetration constraints, thereby modelling both free-space and constrained dynamics in a single set of equations, this work does not require a single set of equations.

The contact state is then a discrete variable $n \in [1, \dots, N]$, where each contact state n has a corresponding constraint $\phi_n(q) = 0$. This constraint can be eliminated, subject to some technical conditions [35], to give the effective coupled dynamics in each contact mode.

2.3 Observation model

Denote a position measurement at time step t which measures a subset of positions $\theta_t \in \Theta \subset Q$, representing, e.g. that only the motor positions are measured.

Let the measured torques/forces $f_t \in \mathbb{R}^L$ be a subset of the forces on compliant elements,

$$\mathbf{f}_t = K_f^n(q_t) + \epsilon_t \quad (2)$$

where $\epsilon_t \sim \mathcal{N}(0, \Sigma_f)$ is i.i.d. noise capturing electrical or quantisation noise, and $K_f^n : Q \rightarrow \mathbb{R}^L$ the effective sensor stiffness for the mode n . As force/torque sensors measure displacement – either strain or bulk displacement [36] – practical force measurements can be captured in (2), given a proper choice of Q .

3 Contact Information Gain

Bayesian inference is used to infer contact state given a prior belief of contact mode, position and force measurements. The prior distribution can reflect a priori assumptions about the environment, e.g., that a contact occurs at a certain location, or it could be a belief informed by other sensors.

3.1 Fully Observed

When the system is fully observed, i.e. $\Theta = Q$, consider a prior belief $p(n)$, and the belief after a measurement f, θ :

$$p(n|f, \theta) = \frac{p(f|n, \theta)p(n)}{\sum_{m=1}^N p(f|m, \theta)p(m)}, \quad (3)$$

where the denominator is a normalization constant.

In the fully observed case, multiple measurements are independent, and the full posterior is

$$p(n|f_{1:t}, \theta_{1:t}) \propto p(n) \prod_{i=1}^t p(f_i|n, \theta_i). \quad (4)$$

3.2 Partially observed

In the partially observed case, some elements of Q are not directly measured, so we denote measured position θ_t and unmeasured position \bar{q}_t , where $q_t = [\theta_t^T, \bar{q}_t^T]^T$, making the force observation model $p(f_t|\bar{q}_t, \theta_t, n)$. A dynamic model such as a discretized version of (1) can be used for inference, where the dynamics $p(\bar{q}_{t+1}|\bar{q}_t, \theta_t, n)$ are known, allowing a standard recursive estimate of

$$\begin{aligned} & p(\bar{q}_t|\theta_{1:t-1}, f_{1:t-1}, n) \\ & \propto \int p(\bar{q}_1) \prod_{i=1}^{t-1} p(\bar{q}_{i+1}|\bar{q}_i, \theta_i, n) p(f_i|\bar{q}_i, \theta_i, n) \bar{q}_{1:t-1}, \end{aligned} \quad (5)$$

where $p(\bar{q}_1)$ is an initial distribution of \bar{q} . In the linear case, a Kalman filter can be used to calculate the posterior on \bar{q}_t . In the nonlinear flexible-joint robot case, various observers of load-side position/velocity are established [33].

The observation model (2) then needs to be marginalized over the uncertain \bar{q}_t as

$$p(f_t|n, f_{1:t-1}, \theta_{1:t}) = \int p(f_t|n, \bar{q}_t, \theta_t) p(\bar{q}_t|f_{1:t-1}, \theta_{1:t-1}, n) d\bar{q}_t. \quad (6)$$

If the force observations (2) are linear, i.e. $K_f^n(q_t) = K_f^n(q_t - q_0^n)$ where $K_f^n \in \mathbb{R}^{L \times D}$ and q_0^n is the rest position of the spring. Denote the posterior belief of $p(q_t|n, f_{1:t-1}, \theta_{1:t-1}) = \mathcal{N}(\mu_q^n, \Sigma_q^n)$ (with a slight abuse of notation, as the θ elements of q have zero uncertainty), then the closed-form marginalized distribution is

$$p(f_t|n, f_{1:t-1}, \theta_{1:t-1}) = \mathcal{N}(K_f^n(\mu_q^n - q_0^n), K_f^n \Sigma_q^n K_f^{n,T} + \Sigma_f). \quad (7)$$

Note that the covariance in f_t now depends on the uncertainty in the configuration q_t and the stiffness K_f^n in addition to force sensor noise Σ_f .

3.3 Information gain

The information gain is proposed as the change in belief entropy, i.e. how much an observation changes the uncertainty. Recall that entropy measures the degree of uncertainty in a discrete random variable $H(\mathbf{n}) = -\sum_{n=1}^N p(n) \ln(p(n))$ and differential entropy over continuous random variables $h(\mathbf{x}) = -\int p(x) \ln p(x) dx$ [37], we define the information gain as

$$\Delta_I = H(\mathbf{n}) - H(\mathbf{n}|\mathbf{f}, \theta). \quad (8)$$

A larger Δ_I means that the measurement brings more certainty. Note that Δ_I depends on the system state, the prior distribution $p(n)$, and the observation model.

Denoting a belief vector $b \in \mathbb{R}^N$, where $p(n) = b_n, b_n > 0, \|b\|_1 = 1$, and the distribution of \mathbf{f} per mode as

$$p(f|n, \theta) = \mathcal{N}(f|\mu_n, \Sigma_n), \quad (9)$$

the following relations hold:

$$H(\mathbf{n}|\mathbf{f}, \theta) = H(\mathbf{n}) - h(\mathbf{f}|\theta) + h(\mathbf{f}|\mathbf{n}, \theta), \quad (10)$$

$$h(\mathbf{f}|\mathbf{n}, \theta) = \frac{L}{2} \ln 2\pi e + \sum_n \frac{b_n}{2} \ln \det \Sigma_n, \quad (11)$$

$$h(\mathbf{f}|\theta) \geq - \sum_n b_n \ln \left(\sum_m b_m \mathcal{N}(\mu_m|\mu_n, \Sigma_n + \Sigma_m) \right), \quad (12)$$

where (10) results from writing $I(\mathbf{f}, \mathbf{n}|\theta)$ two ways, $h(\mathbf{f}|\theta) - h(\mathbf{f}|\mathbf{n}, \theta) = H(\mathbf{n}|\theta) - H(\mathbf{n}|\mathbf{f}, \theta)$ [38], (11) is standard multivariate Gaussian entropy with the expectation taken over \mathbf{n} [37], and (12) is directly Theorem 2 of [39]. Then, Δ_I can be lower bounded as $\Delta_I \geq \underline{\Delta}_I$ where

$$\begin{aligned} \underline{\Delta}_I = & - \sum_n b_n \ln \sum_m b_m \mathcal{N}(\mu_n|\mu_m, \Sigma_n + \Sigma_m) \\ & - \frac{L}{2} \ln 2\pi e - \sum_n \frac{b_n}{2} \ln \det \Sigma_n. \end{aligned} \quad (13)$$

To demonstrate, the information gain bound $\underline{\Delta}_I$ for $N = 2$, $L = 1$, and $b_n = 0.5$ is shown in Figure 2, where $\mu_1 = 0$, $\Sigma_1 = 1$, and μ_2, Σ_2 are varied. The minima is reached when $\mu_2 = 0, \Sigma_2 = 1$, where the two distributions are identical. As Σ_2 decreases, the information gain increases, as well as when $|\mu_2 - \mu_1|$ increases. Note that the information gain saturates - the maximum reduction in uncertainty is the prior uncertainty $H(\mathbf{n})$.

In the partially-observed case, $\underline{\Delta}_I = H(\mathbf{n}) - H(\mathbf{n}|\mathbf{f}_t, f_{1:t-1}, \theta_{1:t})$, modifying the per mode force distributions (9).

4 Information flow in two-mass systems

In this section, information gain is considered on a linear, inertial system as seen in Figure 3. We consider that force is measured as $f_t = K_1(q^2 - q^1) + \epsilon_t$, where $\epsilon_t \sim \mathcal{N}(0, \Sigma_f)$.

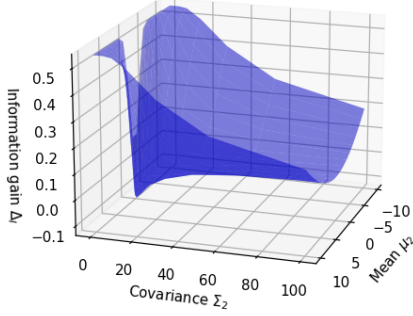


Figure 2: Information gain for single observation with two modes, where $\mu_1 = 0$, $\Sigma_1 = 1$. As the differences between the two distributions increase, the information gain increases, and the mode can be more accurately inferred.

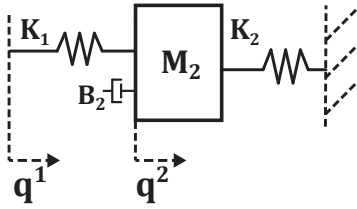


Figure 3: Linear inertial model, where q_1 is measured robot or motor position, and q_2 possibly unmeasured.

Consider the two modes of free space, where $K_1 = 0$, and contact with M_2 where $K_1 > 0$. This gives

$$\begin{aligned} p(f|n=1) &= \mathcal{N}(0, \Sigma_f) \\ p(f|n=2, q^1, q^2) &= \mathcal{N}(K_1(q^1 - q^2), \Sigma_f). \end{aligned} \quad (14)$$

4.1 Fully observed

In the fully observed case, the positions of q^1, q^2 are known a priori or directly measured. If we consider the information gain at a flat prior $b_n = 0.5$, (13) can be used with (14) to find

$$\begin{aligned} \Delta_I(q^1, q^2) &= -\ln(\mathcal{N}(0|K_1(q^1 - q^2), 2\Sigma_f)) \\ &\quad - \frac{1}{2}\ln 2\pi e - \frac{1}{2}\ln \Sigma_f \end{aligned} \quad (15)$$

$$= \frac{1}{2}K_1^2(q^1 - q^2)^2(2\Sigma_f)^{-1} - \frac{1}{2}(1 - \ln 2), \quad (16)$$

using $\mathcal{N}(\mu_n|\mu_m, \Sigma_n + \Sigma_m) = \mathcal{N}(\mu_m|\mu_n, \Sigma_n + \Sigma_m)$.

Here, we note that the information flow increases as K_1 does, $|q^1 - q^2|$ grows, or as Σ_f decreases, i.e. sensor noise decreases.

4.2 Partially observed

As time is relevant in the partially observed case, we denote q_t^1 and q_t^2 as the values at time step t , and consider that q_t^1 is

measured, along with force as in (14). In this case, first-order discretized system dynamics can be written as

$$\begin{aligned} \begin{bmatrix} q_{t+1}^2 \\ \dot{q}_{t+1}^2 \end{bmatrix} &\approx \begin{bmatrix} 1 & T_s \\ -T_s \frac{K_2 + K_1}{M_2} & 1 - T_s \frac{B_2}{M_2} \end{bmatrix} \begin{bmatrix} q_t^2 \\ \dot{q}_t^2 \end{bmatrix} \\ &\quad + \begin{bmatrix} 0 \\ T_s M_2^{-1} K_1 \end{bmatrix} q_t^1 + \begin{bmatrix} 0 \\ M_2^{-1} \end{bmatrix} \mathbf{w}_t \\ &= A \begin{bmatrix} q_{t+1}^2 \\ \dot{q}_{t+1}^2 \end{bmatrix} + B q_t^1 + B_w \mathbf{w}_t \end{aligned} \quad (17)$$

where $\mathbf{w}_t \sim \mathcal{N}(0, \Sigma_w)$ is i.i.d. process noise which is assumed to be a force disturbance, and thus multiplied by M_2^{-1} .

A Kalman estimator can be written, where, for simplicity, we consider the covariance of $p(q_t^2|f_{1:t}, q_{1:t}^1)$ as $t \rightarrow \infty$, which is given by the steady-state covariance of P , which satisfies the discrete algebraic Riccati equation of

$$P = APA^T - APC^T(CPC^T + \Sigma_f)^{-1}CPA^T + B_w \Sigma_w B_w^T. \quad (18)$$

where A, B and B_w are from (17) and $C = [K_1, 0]$ [40].

While the steady-state covariance P is not necessarily the covariance during transient phases (i.e. when starting from an uncertain initial condition), it has a simple closed-form solution which is differentiable [41].

With this assumption, $p(q_t^2|f_{1:t-1}, q_{1:t-1}^1) \sim \mathcal{N}(\mu_t^2, P^+)$, where $P^+ = APA^T + B_w \Sigma_w B_w^T$ and the posterior distribution on \mathbf{f}_t can be written as:

$$\begin{aligned} p(f_t|n=2, q_{1:t}^1, f_{1:t-1}) &= \\ \mathcal{N}(K_1(\mu_t^2 - q_t^1), K_1 P^+ K_1^T + \Sigma_f), \end{aligned} \quad (19)$$

updating the contact force distribution in (14).

5 Experimental Results

We test the validity of information gain in experiments with industrial robots (7 and 60 Kg payload) and varying compliant conditions. A F/T sensor is integrated at the flange and measured at 1250 Hz, and position commands are sent to the robot at 1250 Hz, allowing the realization of standard admittance control and collision detection. When collision is detected, the position commanded to the robot is held to the last position before collision was detected. The F/T sensors used in all setups have similar noise properties, and $\Sigma_f = 1.25$ is used for all conditions.

The experimental data and analysis code is available at <https://owncloud.fraunhofer.de/index.php/s/ovt01GRb7o7b9Fb>.

5.1 Monitoring Assembly

To investigate the impact on more complex tasks, we consider an admittance-controlled gear assembly task from [31], where the gear assembly has multiple stages, as seen in Figure 1. One failure mode is in-hand slip, which may occur during the gear mating process. We modify the setup by introducing additional foam at the fingertips, between the gripper and

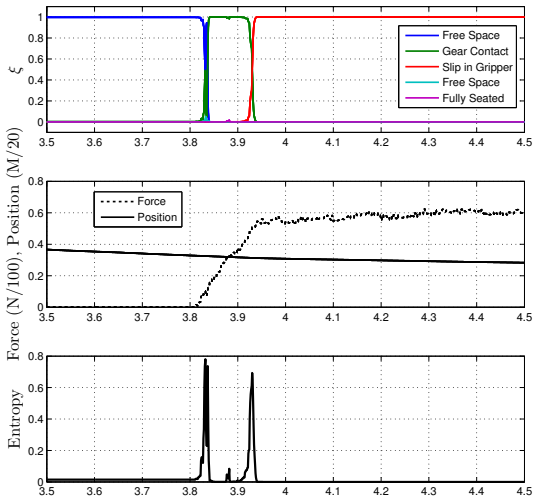


Figure 4: Detail of transition in mode estimate, with estimated contact state over time (top), force/position (middle) and belief entropy at each time step (bottom).

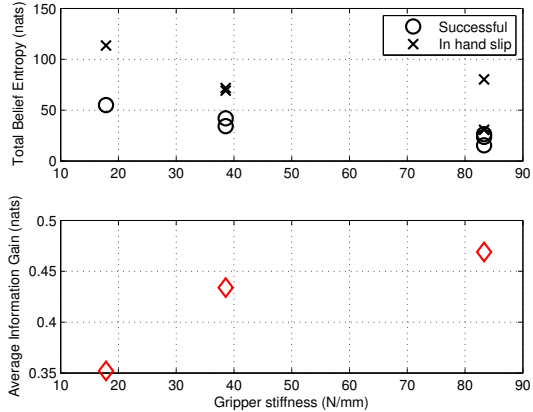


Figure 5: Total belief entropy over compliance at the gripper. For both successful and in hand slip trials, the uncertainty increases as the compliance decreases.

gear, and compare the ability to infer the task mode. The parameters of the estimator are available with the experimental data in the above mentioned cloud folder.

A typical mode detection from a trial with in-hand slip can be seen in Figure 4, where the belief entropy increases substantially during the transitions between the modes. Comparing the total entropy over a number of experiment iterations, we find that decreasing the gripper stiffness increases the sum of entropy, as seen in Figure 5.

The information gain is calculated using the fully-observed information gain (16) with the gripper stiffness as K_1 , and the average taken over $|q_1 - q_2| \in [0, 0.5]$ mm with a flat prior $b_n = 1/N$. It can be seen that the higher stiffness has higher information gain, corresponding with lower total belief entropy.

5.2 Collision detection - High Payload Robot

A 16 Kg plate is mounted to a large industrial robot as seen in Figure 7, and brought into contact with a compliant magazine,

Condition	K_1	M_2	B_2	K_2	Δ_I
Flex Joints	17.4e4	20.1	305	2630	0.131
Compliant Surface	1.3e4	63.9	1870	7350	0.0743
Compliant Feet	2.61e4	69.3	1080	1.81e4	0.348
Flex Joints Gradient	7.7e-6	7.6e-3	2.2e-6	-4.8e-10	-
Comp Surf Gradient	1.5e-5	1.8e-3	1.7e-6	1.3e-10	-
Comp Feet Gradient	2.5e-5	0.8e-3	1.3e-6	4.8e-10	-

Table 1: Identified dynamic parameters for the magazine contact

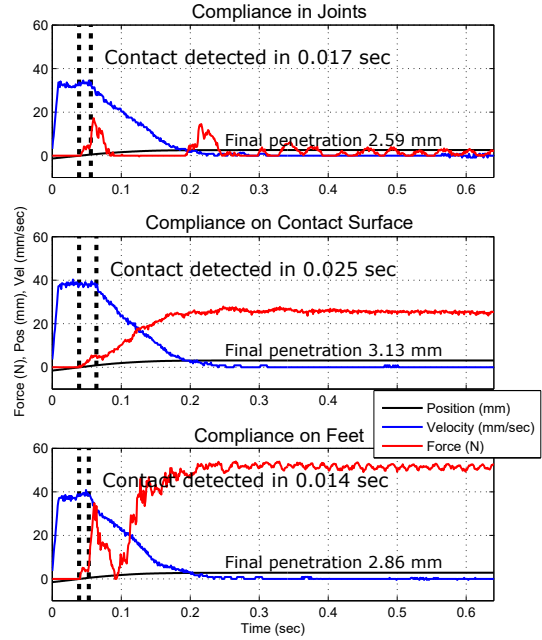


Figure 6: Contact force, position, and velocity in experiments with the contact detection

where compliance is introduced in one of three locations: (i) in the joints of the magazine, (ii) on the contact surface, and (iii) under the feet of the magazine. The robot was driven into contact in using force control with a desired contact force of 30 N. Pure admittance control is used for model identification, than contact detection is activated, where a simple force threshold of 6 N is used (gravitational forces of the plate are compensated).

As seen in Figure 6, the fastest contact detection occurred with compliance on the feet (bottom), where the hard contact and larger effective magazine inertia results in an initial peak in force. Compliance in the joints results in the 2nd fastest contact detection – note that in this case contact was lost as the magazine springs back with the lower K_2 . The slowest contact detection was with compliance at the contact surface, where force builds more slowly.

A model for these three compliance cases is then identified following the inertial model in Figure 3, where the measured position is q^1 and the measured force is that on K_1 . These parameters are identified by doing a least-squares fit $\min_{K_1, M_2, B_2, K_2} \sum_t \|f_t^m - f_t\|$, where f_t^m is the model output given the observed q_t^1 as input, and can be seen in Table 1, with time plots in Figure 8.

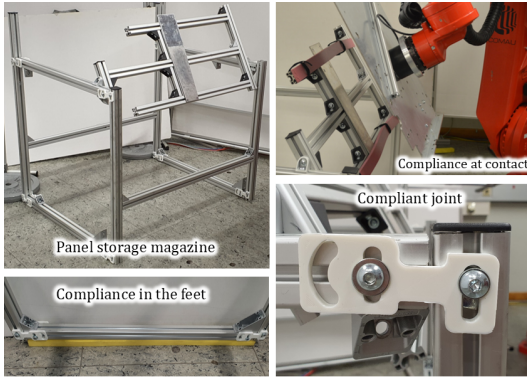


Figure 7: Contact magazine with the various locations of compliance, using strips of viscoelastic foam, or 3d printed flexure joints.

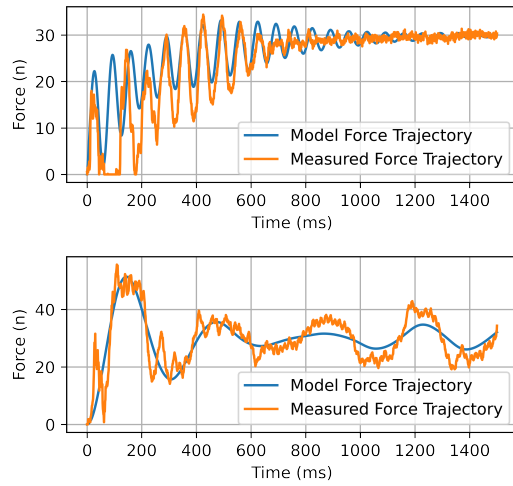


Figure 8: Identified model and real response, for flex joint magazine (top) and compliance in the feet (bottom). Contact is made with force control, with desired force of 30 N.

From these models, the Δ_I can be calculated in the partially observed case with q_t at time $t = 0.002$. It can be seen in Table 1 that the compliant feet has the highest information gain, followed by flex joints and compliant surface, corresponding to the contact detection performance. Because the Δ_I calculation is composed of differentiable operations, the gradient can be numerically calculated with an automatic differentiation toolbox [42], also seen in Table 1. It can be seen that increasing K_1 and M_2 make the largest increase in Δ_I , while B_2 and K_2 play a more minor role.

The gradient validates an experimental observation: although K_1 is higher with the flex joints than in compliant feet case, the lower inertia of M_2 results in lower information gain and longer contact detection time.

5.3 Collision Detection - Medium Payload Robot

A compliant table, seen in Figure 9, was used to investigate the impact of location and quantity of compliance on the ability to detect contact. By varying the compliance in the feet

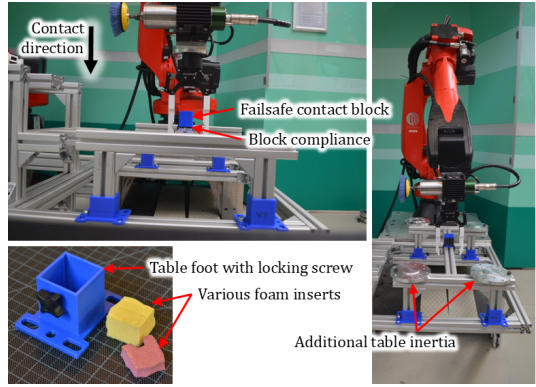


Figure 9: Compliant table with 7 Kg payload robot, where compliance can be adjusted in the feet of the table or between the failsafe block and table.

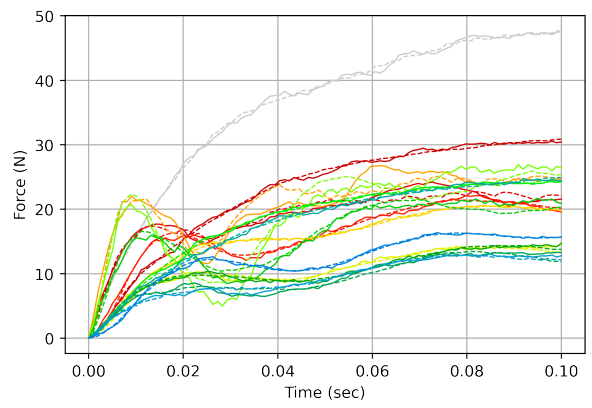


Figure 10: Traces of contact force (solid line) vs identified model response (dotted). Detailed responses can be better seen on the online repository, these responses show the range of force profiles and model fit.

and contact surface, as well as the inertia of the table, a range of contact responses were achieved as seen in Figure 10. A simple contact detection threshold of 6 N was applied, and the performance can be seen in the attached video. Model identification was done as above, but a two-inertia model was found to provide better model fit, requiring a straightforward extension to (17) which is omitted due to space constraints but in the published code.

The information gain, calculated with the partially observed q_t at $t = 0.002$, is compared with the time taken to detect the contact in Figure 11. It can be seen that the information gain has a strong negative correlation with the time taken to detect contact, validating it as a measure of the ability to detect environmental contact.

The configurations where block compliance was removed, and where additional weight was added to the table, had higher information gain and a higher contact velocity could be safely achieved - further detailed plots are available online with the experimental data.

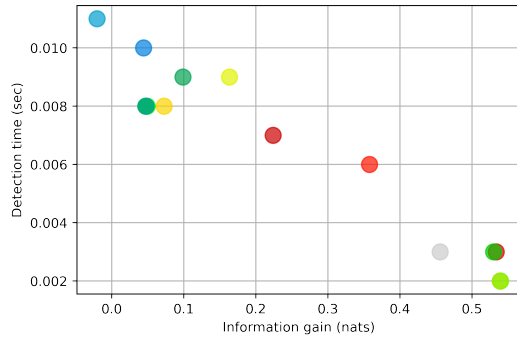


Figure 11: Information gain vs time to detect contact, colors are consistent with those used in Figure 10. As information gain increases, the time required to detect contact decreases.

6 Conclusion

The impact of mechatronic design, especially compliance, on the ability to detect contact conditions was presented, and formalized in a metric of the information gain. This metric is validated to predict the certainty with a complex assembly task can be monitored, and the speed with which collision can be detected.

In the case of introducing compliance to the environment, it is shown that this compliance is best introduced not at the point of contact, but deeper into the kinematic structure. When using contact detection, increasing the contacted inertia allows a faster recognition from the higher transient force.

Information gain was shown to be predictive even when using a simpler contact detection threshold, and has advantages over closed-form expressions for contact force: the Bayesian framework allows it to be integrated with other sensors and estimators, and as it is differentiable, it can be efficiently optimized or the gradient inspected for insight to the impact of dynamic parameters.

References

- [1] M. Baum and O. Brock, "Achieving robustness by optimizing failure behavior," in *2017 IEEE International Conference on Robotics and Automation (ICRA)*, May 2017, pp. 5806–5811.
- [2] M. Vecerik, *et al.*, "A Practical Approach to Insertion with Variable Socket Position Using Deep Reinforcement Learning," *arXiv:1810.01531 [cs]*, Oct. 2018.
- [3] D. E. Stewart, "Rigid-Body Dynamics with Friction and Impact," *SIAM Review*, vol. 42, no. 1, pp. 3–39, Jan. 2000.
- [4] R. Tedrake, "Underactuated Robotics: Algorithms for Walking, Running, Swimming, Flying, and Manipulation (Course Notes for MIT 6.832)," *Downloaded on October 2020 from http://underactuated.mit.edu*, 2020.
- [5] E. Todorov, "A convex, smooth and invertible contact model for trajectory optimization," in *2011 IEEE International Conference on Robotics and Automation*, May 2011, pp. 1071–1076.
- [6] A. M. Castro, *et al.*, "A Transition-Aware Method for the Simulation of Compliant Contact With Regularized Friction," *IEEE Robotics and Automation Letters*, vol. 5, no. 2, pp. 1859–1866, Apr. 2020.
- [7] M. Toussaint, J.-S. Ha, and D. Driess, "Describing Physics For Physical Reasoning: Force-based Sequential Manipulation Planning," *arXiv:2002.12780 [cs]*, Feb. 2020.
- [8] F. Wirnshofer, *et al.*, "Robust, Compliant Assembly via Optimal Belief Space Planning," in *2018 IEEE International Conference on Robotics and Automation (ICRA)*, May 2018, pp. 1–5.
- [9] S. Pfrommer, M. Halm, and M. Posa, "Contact-Nets: Learning of Discontinuous Contact Dynamics with Smooth, Implicit Representations," *arXiv preprint arXiv:2009.11193*, 2020.
- [10] M. A. Lee, *et al.*, "Making Sense of Vision and Touch: Learning Multimodal Representations for Contact-Rich Tasks," *IEEE Transactions on Robotics*, vol. 36, no. 3, pp. 582–596, June 2020.
- [11] J. Xu, *et al.*, "Compare Contact Model-based Control and Contact Model-free Learning: A Survey of Robotic Peg-in-hole Assembly Strategies," *arXiv:1904.05240 [cs]*, Apr. 2019.
- [12] N. Hogan, "Impedance Control: An Approach to Manipulation: Part II—Implementation," *Journal of Dynamic Systems, Measurement, and Control*, vol. 107, no. 1, pp. 8–16, Mar. 1985.
- [13] P. M. Wensing, *et al.*, "Proprioceptive Actuator Design in the MIT Cheetah: Impact Mitigation and High-Bandwidth Physical Interaction for Dynamic Legged Robots," *IEEE Transactions on Robotics*, vol. 33, no. 3, pp. 509–522, June 2017.
- [14] S. Haddadin, A. Albu-Schaeffer, and G. Hirzinger, "Safety Evaluation of Physical Human-Robot Interaction via Crash-Testing," *Robotics: Science and Systems Foundation*, June 2007.
- [15] A. Bicchi and G. Tonietti, "Fast and "Soft-Arm" Tactics," *IEEE Robotics & Automation Magazine*, vol. 11, no. 2, pp. 22–33, June 2004.
- [16] K. Haninger and D. Surdilovic, "Bounded Collision Force by the Sobolev Norm: Compliance and Control for Interactive Robots," in *2019 IEEE International Conference on Robotics and Automation (ICRA)*, 2019, pp. 8259–8535.
- [17] S. D. Eppinger and W. P. Seering, "Three dynamic problems in robot force control," *IEEE Transactions on Robotics and Automation*, vol. 8, no. 6, pp. 751–758, 1992.
- [18] G. Pratt and M. Williamson, "Series elastic actuators," in *1995 IEEE/RSJ International Conference on Intelligent Robots and Systems 95. 'Human Robot Interaction and Cooperative Robots', Proceedings*, vol. 1, Aug. 1995, pp. 399–406 vol.1.
- [19] P. Tomei, "A simple PD controller for robots with elastic joints," *Automatic Control, IEEE Transactions on*, vol. 36, no. 10, pp. 1208–1213, 1991.
- [20] H. Vallery, *et al.*, "Compliant actuation of rehabilitation robots," *Robotics & Automation Magazine, IEEE*, vol. 15, no. 3, pp. 60–69, 2008.
- [21] C. Della Santina, *et al.*, "Controlling Soft Robots: Balancing Feedback and Feedforward Elements," *IEEE Robotics Automation Magazine*, vol. 24, no. 3, pp. 75–83, Sept. 2017.
- [22] E. A. Bolivar-Nieto, *et al.*, "Convex Optimization for Spring Design in Series Elastic Actuators: From Theory to Practice," 2021.
- [23] S. Haddadin, *et al.*, "Exploiting elastic energy storage for "blind" cyclic manipulation: Modeling, stability analysis, control, and experiments for dribbling," *IEEE Transactions on Robotics*, vol. 34, no. 1, pp. 91–112, 2018.
- [24] V. C. Müller and M. Hoffmann, "What Is Morphological Computation? On How the Body Contributes to Cognition and Control," *Artificial Life*, vol. 23, no. 1, pp. 1–24, Jan. 2017.
- [25] A. Mo, *et al.*, "Effective Viscous Damping Enables Morphological Computation in Legged Locomotion," *arXiv:2005.05725 [cs]*, May 2020.
- [26] K. Haninger, "Minimum directed information: A design principle for compliant robots," in *IEEE International Conference on Robotics and Automation (ICRA)*, 2021.

- [27] M. Hamaya, *et al.*, “Learning robotic assembly tasks with lower dimensional systems by leveraging physical softness and environmental constraints,” in *2020 IEEE International Conference on Robotics and Automation (ICRA)*. IEEE, 2020, pp. 7747–7753.
- [28] M. P. Polverini, A. M. Zanchettin, and P. Rocco, “A constraint-based programming approach for robotic assembly skills implementation,” *Robotics and Computer-Integrated Manufacturing*, vol. 59, pp. 69–81, 2019.
- [29] I. F. Jasim and P. W. Plapper, “Contact-state recognition of compliant motion robots using expectation maximization-based Gaussian mixtures,” in *ISR/Robotik 2014; 41st International Symposium on Robotics; Proceedings Of*. VDE, 2014, pp. 1–8.
- [30] T. Ren, *et al.*, “Collision detection and identification for robot manipulators based on extended state observer,” *Control Engineering Practice*, vol. 79, pp. 144–153, 2018.
- [31] K. Haninger and D. Surdilovic, “Multimodal Environment Dynamics for Interactive Robots: Towards Fault Detection and Task Representation,” in *Proc. IEEE/RSJ Intl Conf on Intelligent Robots and Systems (IROS)*, 2018, pp. 6932–6937.
- [32] T. J. Debus, P. E. Dupont, and R. D. Howe, “Distinguishability and identifiability testing of contact state models,” *Advanced Robotics*, vol. 19, no. 5, pp. 545–566, 2005.
- [33] S. Haddadin, A. De Luca, and A. Albu-Schäffer, “Robot collisions: A survey on detection, isolation, and identification,” *IEEE Transactions on Robotics*, vol. 33, no. 6, pp. 1292–1312, 2017.
- [34] M. W. Spong, “Modeling and control of elastic joint robots,” *Journal of dynamic systems, measurement, and control*, vol. 109, no. 4, pp. 310–318, 1987.
- [35] E. Shmoyslova, *et al.*, “Simplification of Differential Algebraic Equations by the Projection Method1,” p. 10.
- [36] N. Kashiri, J. Malzahn, and N. G. Tsagarakis, “On the Sensor Design of Torque Controlled Actuators: A Comparison Study of Strain Gauge and Encoder-Based Principles,” *IEEE Robotics and Automation Letters*, vol. 2, no. 2, pp. 1186–1194, Apr. 2017.
- [37] T. M. Cover, *Elements of Information Theory*. John Wiley & Sons, 1999.
- [38] A. Kolchinsky and B. D. Tracey, “Estimating mixture entropy with pairwise distances,” *Entropy*, vol. 19, no. 7, p. 361, 2017.
- [39] M. F. Huber, *et al.*, “On entropy approximation for Gaussian mixture random vectors,” in *2008 IEEE International Conference on Multisensor Fusion and Integration for Intelligent Systems*. IEEE, 2008, pp. 181–188.
- [40] S. Thrun, “Probabilistic robotics,” *Communications of the ACM*, vol. 45, no. 3, pp. 52–57, 2002.
- [41] T.-C. Kao and G. Hennequin, “Automatic differentiation of Sylvester, Lyapunov, and algebraic Riccati equations,” *arXiv:2011.11430 [cs, math]*, Nov. 2020.
- [42] J. A. Andersson, *et al.*, “CasADi: A software framework for nonlinear optimization and optimal control,” *Mathematical Programming Computation*, vol. 11, no. 1, pp. 1–36, 2019.